RSC Chemical Biology

ROYAL SOCIETY OF CHEMISTRY

PAPER

View Article Online
View Journal | View Issue

Check for updates

Cite this: *RSC Chem. Biol.*, 2023, 4, 592

An anti-glioblastoma gold(I)–NHC complex distorts mitochondrial morphology and bioenergetics to induce tumor growth inhibition†

Charles E. Greif,[a] R. Tyler Mertens,[a] Gilles Berger,[bc] Sean Parkin[a] and Samuel G. Awuah*[ade]

Received 8th April 2023,
Accepted 19th May 2023

DOI: 10.1039/d3cb00051f

rsc.li/rsc-chembio

Glioblastoma multiforme (GBM) is the most lethal brain cancer subtype, often advanced by the time of initial diagnosis. Existing treatment modalities including surgery, chemotherapy and radiation have been stymied by recurrence, metastasis, drug resistance and brain targetability. Here, we report a geometrically distinct Au(I) complex ligated by N^N-bidentate ligands and supported by a N-heterocyclic ligand that modulates mitochondrial morphology to inhibit GBM *in vitro* and *in vivo*. This work benefits from the facile preparation of anti-GBM Au(I)-NHC complexes.

Introduction

Glioblastoma multiforme (GBM) is the most aggressive and commonly diagnosed cancer type of the central nervous system with an average length of patient survival estimated to be only 8 months.[1,2] Current therapeutic regimens such as surgery, radiation, and chemotherapy target bulk tumors and impose toxic side effects on normal cells. A more quiescent cell population known as cancer stem cells with high dependence on mitochondrial oxidative phosphorylation may be culpable in GBM resistance, evasion, metastasis, and lethality.[3–5] Additionally, aggressive tumor types have elevated mitochondrial fusion and fission activity referred to as mitochondrial dynamics that support high proliferation and invasiveness.[6–8]

The number of mitochondria ranging from several to thousands characterizes the metabolic activity of different cell types.[9,10] The mitochondria in metabolically active cells including the brain, gametes, hepatocytes and cardiomyocytes comprise ~20–30% of the cell volume.[11] A crucial element that controls the function, morphology, organizational clearance, and population of mitochondria is fusion/fission dynamics.[12,13] Mitochondria consist of a double membrane system, with the inner membrane containing a multitude of cristae and the outer membrane consisting of various porins to allow the influx of ions and other uncharged molecules.[14] The opposing but well-coordinated mitochondrial fusion and fission events are mediated by mitofusins (MFN1 and MFN2 in mammals) for outer membrane fusion, and large GTPases of the dynamin family (DRP1) for fission on the outer membrane.[8,12,15] Another dynamin family member embedded in the inner membrane for fusion is optic atrophy 1 (OPA1).[8,12,15] Cancer progression is characterized by enhanced fission or fusion activity, therefore presenting therapeutic vulnerability.[12,13]

Gold complexes have shown tremendous promise in the clinic and preclinically[16–21] for inducing immunogenic cell death,[22] as anticancer,[17,23] antileishmanial,[24] and antibacterial agents,[25] and for irritable bowel disease,[26] among others;[27,28] however, they have not, to the best of our knowledge, been investigated as perturbants of mitochondrial dynamics in GBM. Fruitful structure activity relationship studies that guide the discovery of probes and therapeutics that target mitochondrial dynamics are lacking. Au(I) and Au(III) complexes commonly inhibit thiol-containing enzymes, specifically glutathione (GSH) and thioredoxin reductase, the mitochondria, and various deubiquitinases.[29,30] To overcome the current limitations of gold-based anticancer agents regarding potency, defined mechanisms of action, and stability, we and others have developed novel Au(I) and Au(III) complexes targeting distinct mitochondrial processes including oxidative phosphorylation (OXPHOS), redox homeostasis and more recently structure.[9,23,31–33] Here, we report a rationally designed gold(I) complex that distorts mitochondrial morphology to inhibit GBM tumor growth *in vitro* and *in vivo*.

[a] *Department of Chemistry, University of Kentucky, Lexington, Kentucky 40506, USA. E-mail: awuah@uky.edu*
[b] *Harvey Cushing Neuro-Oncology Laboratories, Department of Neurosurgery, Brigham and Women's Hospital, Harvard Medical School, Boston, MA 02115, USA*
[c] *Microbiology, Bioorganic & Macromolecular Chemistry, Faculté de Pharmacie, Université libre de Bruxelles (ULB), Boulevard du Triomphe, 1050 Brussels, Belgium*
[d] *Department of Pharmaceutical Sciences, College of Pharmacy, University of Kentucky, Lexington, Kentucky 40536, USA*
[e] *University of Kentucky Markey Cancer Center, University of Kentucky, Lexington, KY, 40536, USA*

† Electronic supplementary information (ESI) available: Detailed experimental and crystallographic data. CCDC 2253712–2253716. For ESI and crystallographic data in CIF or other electronic format see DOI: https://doi.org/10.1039/d3cb00051f

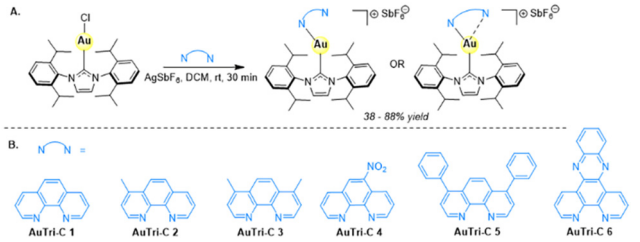

Scheme 1 Chemical structures of AuTri–C complexes. (A) Synthetic scheme for the preparation of Au(I)-NHC compounds in this study. (B) SAR library influenced by diverse [N^N]-bidentate donor ligands.

We believe that our strategy provides a novel path to designing mitochondrial dynamics probes and targeted therapeutics to inhibit aggressive cancer growth.

Results and discussion

Rationale, synthesis, and characterization of AuTri–C complexes

Inspired by our previous work that demonstrated the utility of a three-coordinate Au(I) complex as a disruptor of the mitochondrial structure,[9] we sought to enhance the stability and anticancer potential of such novel structural motif in biology through carbene stabilization. The new class of complexes created consists of diverse [N^N]-bidentate donors ligated to the Au(I) center and an N-heterocyclic carbene (NHC) supporting framework to yield cationic Au(I) complex existing as pseudo-linear or three-coordinate constructs. These tricoordinate Au complexes can yield an asymmetric structure with differing gold–nitrogen bond lengths. The longer Au–N bond is more labile, potentially acting as a coordination site for use in biological systems upon bond breakage. We hypothesize that these tricoordinate gold complexes will selectively target mitochondrial pathways in glioblastoma cell lines given their lipophilic cationic character. Preparation of the Au(I) NHCs, herein referred to as AuTri–C followed a streamlined method that is easy and scalable as shown in Scheme 1. Briefly, Au(I)-NHC complexes synthesized using established methods[34–37] were subjected to a silver transmetalation strategy to install the [N^N]-bidentate donors at the Au(I) center. The complexes were fully characterized by ^{1}H NMR, ^{13}C NMR, and ^{19}F NMR (Fig. S2–S18, ESI†), and purity ascertained by elemental analysis. Structure of the complexes was elucidated by X-ray crystallography.

X-Ray crystallography

Single crystals of **AuTri–C 1–5** were grown by vapor diffusion of diethyl ether into a solution of respective concentrated Au complexes in dichloromethane for analysis by X-ray diffraction to determine the molecular structure (Fig. 1). As shown in Fig. 1A, AuTri–C may exist as a pseudo-linear or three-coordinate structure with one elongated Au–N bond of the overall structure. The selected bond lengths as depicted in Table 1 confirm that the longest Au–N bond length is in the range of 2.634–2.677 Å, which satisfies the parameters of an actual bond. Furthermore, the bond angles confirm a distorted linear geometry around the Au(I) center or a distorted trigonal planar molecular geometry. We posit that the longer Au–N bond is more labile, potentially acting as a coordination site to engage biomacromolecules such as proteins.

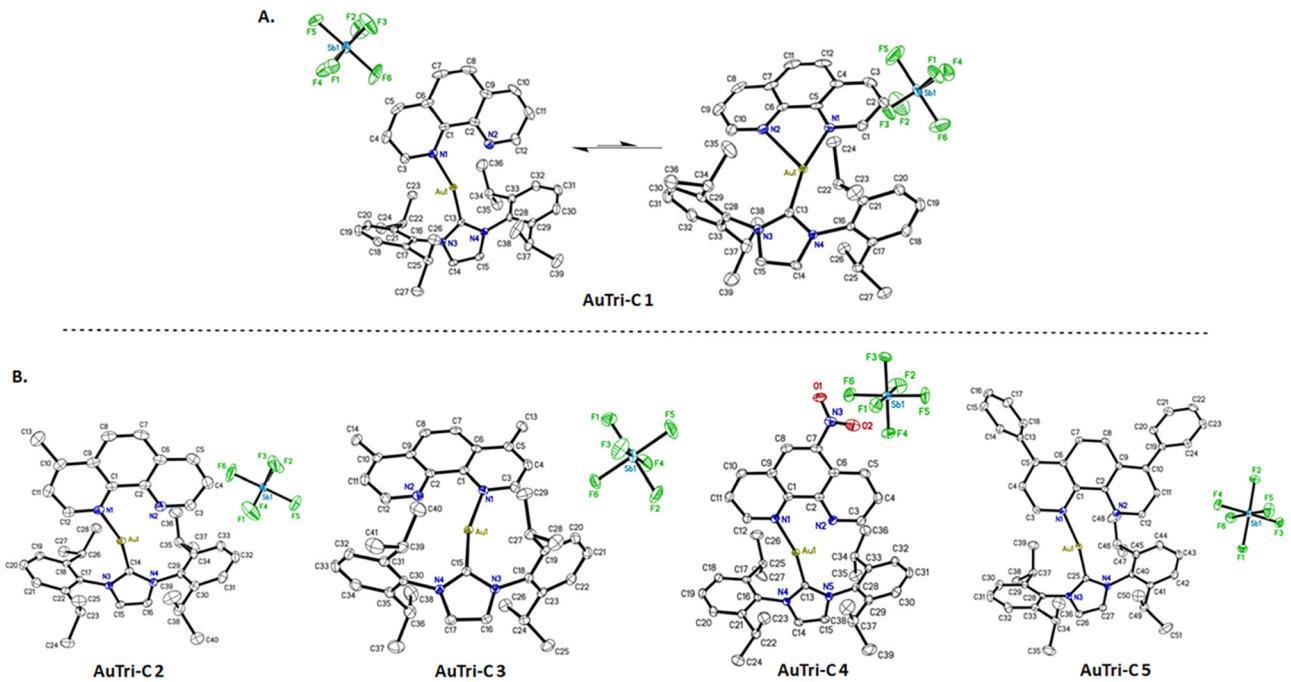

Fig. 1 X-ray crystal structures for AuTri–C complexes. (A) Crystal structure of **AuTri–C 1** showing the transition between two disordered structures: distorted linear (left) and tricoordinate (right). (B) Crystal structures for **AuTri–C 2–5**. Ellipsoids drawn at 50%. Hydrogens and solvent molecules have been omitted for clarity.

Photophysical properties and solution stability

To characterize the photophysical behavior and investigate the solution stability of AuTri–C complexes, DMSO-stock solutions of the complexes were prepared and diluted with Dulbecco's Modified Eagle's Medium (DMEM) for analysis using UV-vis spectrophotometry. A strong high-energy band at 300 nm was observed for **AuTri–C 1–6**. This is attributed to charge transfer transitions. Low energy electronic absorption bands around 400 nm observed could be due to π–π^* transitions from ligand-to-metal charge transfer (LMCT) or metal-to-ligand charge-transfer (MLCT) states. Apart from **AuTri–C 6**, all complexes displayed appreciable solution stability as evidenced by minimal alteration to their electronic bands.

Subsequently, based on the superior stability of **AuTri–C 5** in solution, we further evaluated it in DMSO over a temperature range. Using variable temperature NMR, we found very little change in the ^{1}H-NMR spectra at room temperature or 80 °C (Fig. S19, ESI†), indicating high stability at harsh temperatures. Additionally, incubation of **AuTri–C 5** (5 mM) with 50 mM L-GSH, an abundant biological reductant, did not alter **AuTri–C 5** peaks based on time-dependent ^{1}H-NMR studies at 6 h; however, by 12 h, we noticed an additional peak form next to the methyne peak at 4.34 ppm, characteristic of the oxidation of GSH to GSSG (Fig. S20, ESI†). Reduction to metallic gold was not observed.

The electrochemical behavior of **AuTri–C 3**, **AuTri–C 5**, and **AuTri–C 6** was characterized by cyclic voltammetry in anhydrous acetonitrile with 0.1 M NBu$_4$PF$_6$ as the supporting electrolyte and ferrocenium/ferrocene (Fc/Fc$^+$) redox couple as the standard. Cyclic voltammograms were obtained at 100 mV s^{-1} and is referenced to Ag/AgCl. In complex **AuTri–C 3**, minimal reduction events were observed, but an uncharacteristic oxidation peak at 0.2 V was dominant (Fig. S23, ESI†). We found that **AuTri–C 5** exhibits a characteristic quasi-reversible peak close to −1.5 V (Fig. 2B). Using appropriate controls (Fig. S21–S30, ESI†), the reversible redox behavior is attributed to the overall Au(I) complex. With regards to **AuTri–C 6**, a reduction peak at −1.0 V and a quasi-reversible peak at −1.3 V (Fig. 2C) was observed, whereas also observing several irreversible oxidation events, attributed to the overall stability of the highly conjugated dppz [N^N]-bidentate ligand.

AuTri–C inhibit GBM cell growth and induce apoptosis

Increasing evidence supports the reliance of glioblastoma growth on mitochondrial functional states and OXPHOS.[38–40] Given the potential for three-coordinate Au(I) complexes to distort the mitochondrial structure,[9] we hypothesized that AuTri–C complexes will be effective against the mitochondria-dependent GBM. Using BT333 – a patient-derived glioblastoma cell line – we profiled the library of **AuTri–C 1–6** for anticancer activity. The complexes displayed promising anticancer effects by MTT assay in the sub-micromolar range as shown in Fig. 3A and B. We found that **AuTri–C 5** bearing the bathophenanthroline donor ligand was more potent at IC_{50} ∼ 1.3 μM. Based on the desirable stability and potency, we prioritized **AuTri–C 5** as our lead complex for further mechanism-of-action studies.

To assess the potential of **AuTri–C 5** to induce apoptosis, we used the dual-staining FITC-labeled Annexin-V/PI flow cytometry assay to quantitatively measure early and late phase apoptosis. Cells undergoing apoptosis display phosphatidyl serine on cell surfaces that can bind to Annexin V. **AuTri–C 5** induced apoptosis in a dose-dependent manner as shown in Fig. 3D and the extrapolated bar graph in Fig. 3C showing 23% apoptosis at 10 μM compared to untreated cells at 4% within 24 h. Taken together, **AuTri–C 5** inhibited GBM cell growth and induced apoptotic cell death.

AuTri–C 5 disrupts mitochondrial morphology and function

Intracellular effects of **AuTri–C 5** were initiated by examining mitochondrial morphology in live cells. Mitochondrial fusion characterized by elongated tubular mitochondrial structures[41,42] and fission as characterized by fragmented structures[43] can be observed using confocal microscopy with MitoTracker staining, which selectively stains live mitochondria in cells. GBM as evidenced in BT333 possess active mitochondria with significant fusion features. Upon treatment with **AuTri–C 5**, we observed the loss of the characteristic tubular mitochondrial morphology and a more fragmented phenotype emerged (Fig. 4). This observation implicates mitochondria as a potential target of AuTri–Cs.

Furthermore, the functional effect of **AuTri–C 5** on the mitochondria was explored by mitochondrial membrane potential (MMP) assay. We measured MMP using TMRE dye in BT 333 cells and found significant depolarization as determined by reduced fluorescence in treated cells by flow cytometry (Fig. 5A). BT333 cells treated with **AuTri–C 5** at both 5 μM and 10 μM diminished TMRE fluorescence response compared to the untreated control and 100 μM of CCCP, a classic uncoupler (Fig. 5B).

Dysfunctional mitochondria are characterized by the excessive production of superoxide anions ($O_2^{\bullet-}$).[44–48] We then explored the effect of **AuTri–C 5** on mitochondrial reactive oxygen species (mtROS). MitoSox red is capable of detecting mtROS in cells by flow cytometry or confocal microscopy.[49] BT333 cells exposed to **AuTri–C 5** demonstrated the generation of mtROS (Fig. 5C and D). We then explored the effect of **AuTri–C 5** on mitochondrial reactive oxygen species (mtROS). MitoSox red is capable of detecting mtROS in cells by flow cytometry or confocal microscopy.[49] BT333 cells exposed to **AuTri–C 5** demonstrated the generation of mtROS (Fig. 5C and D). Given that GBM cell survival depends on functional mitochondria, and that the perturbation of mitochondrial function could significantly hamper cancer cell survival, we sought to elucidate the effect of **AuTri–C 5** on mitochondrial bioenergetics utilizing

Table 1 Selected bond lengths and angles for AuTri–C complexes in the tricoordinate system

	Selected bond lengths in tricoordinate system (Å)			Selected bond angles in tricoordinate system (°)		
Compound	Au–N_1	Au–N_2	Au–C_{13}	N_1–Au–C_{13}	N_2–Au–C_{13}	N_1–Au–N_2
AuTri–C 1	2.105	2.674	1.976	126.58	164.39	69.02
AuTri–C 2	2.111	2.677	1.975	128.21	163.19	68.59
AuTri–C 3	2.109	2.657	1.977	126.39	164.93	69.68
AuTri–C 4	2.109	2.634	1.972	124.77	165.76	69.47
AuTri–C 5	2.100	2.644	1.972	122.48	166.35	68.82

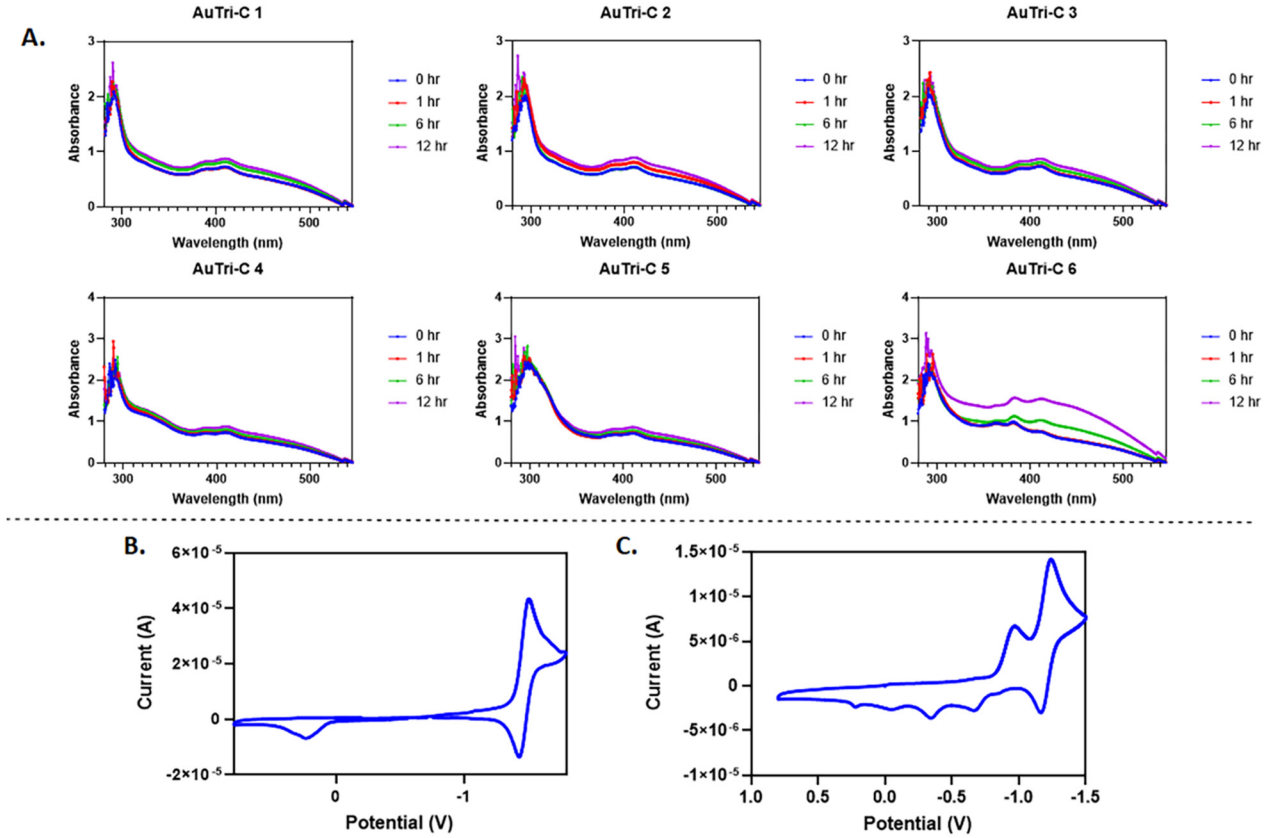

Fig. 2 (A) UV-vis absorption spectra of AuTri–C complexes in biologically relevant media, DMEM at 37 °C, final concentration of the complexes 50 μM. (B and C) Cyclic voltammogram recorded at a platinum electrode in DMSO solution of 5 mM **AuTri–C-5** or **AuTri–C-6** with 0.10 M $N(Bu)_4PF_6$ supporting electrolyte at a scan rate of 0.1 V s^{-1} using Ag/AgCl reference electrode at RT.

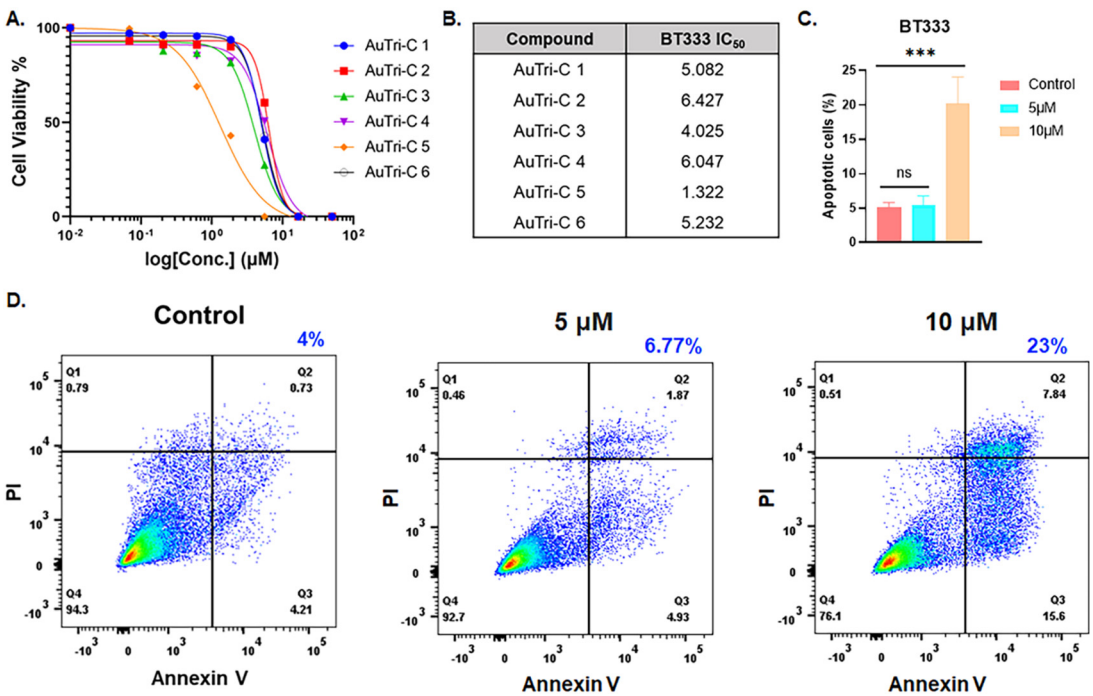

Compound	BT333 IC_{50}
AuTri-C 1	5.082
AuTri-C 2	6.427
AuTri-C 3	4.025
AuTri-C 4	6.047
AuTri-C 5	1.322
AuTri-C 6	5.232

Fig. 3 (A) Cell viability AuTri–C complexes evaluated *via* MTT assay in BT333 Glioblastoma cell line. (B) Table of IC_{50} values extrapolated from Fig. 3A. (C and D) Annexin V-PI assay to assess the impact of **AuTri–C 5** on apoptosis in BT333 Glioblastoma cell line (***$p < 0.001$, ns – not significant).

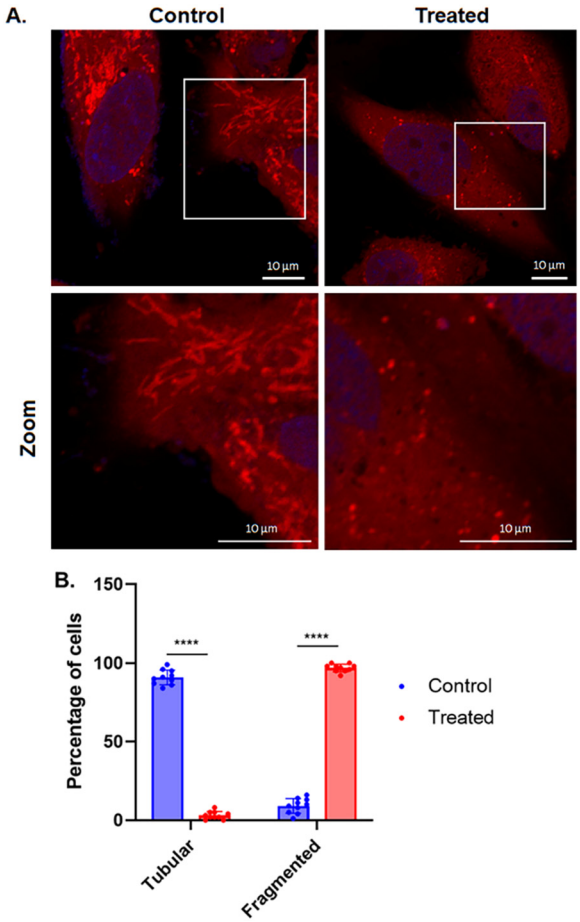

Fig. 4 (A) Confocal microscopy images (original 60× magnification) of mitochondrial morphology of BT333 cells after **AuTri–C 5** treatment. n = 10 cells. Scale bar 10 μm. Red fluorescence – mitochondria; blue fluorescence – DAPI labelled nucleus. **B**. Percentage of cells with tubular and fragmented mitochondria (****$p < 0.0001$).

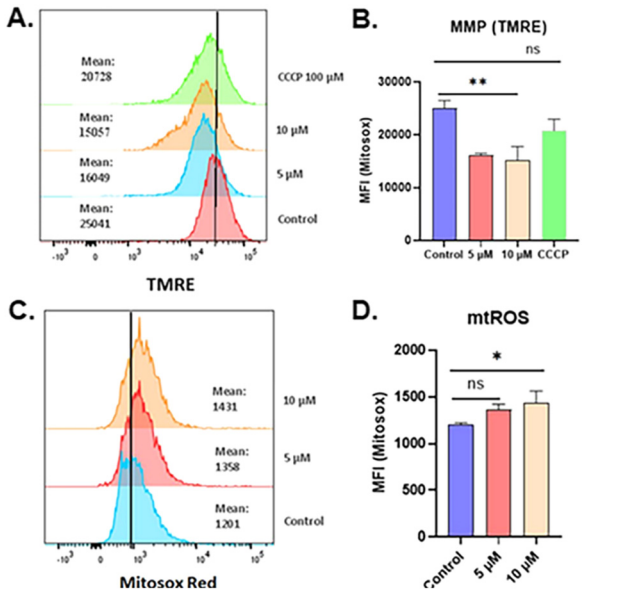

Fig. 5 Mitochondrial perturbation data (A and B). Mitochondrial Reactive Oxygen Species (mtROS) data showing the generation of mtROS after treatment with **AuTri–C 5**. (C and D) Mitochondrial Membrane Potential (MMP) data after treatment with **AuTri–C 5**.

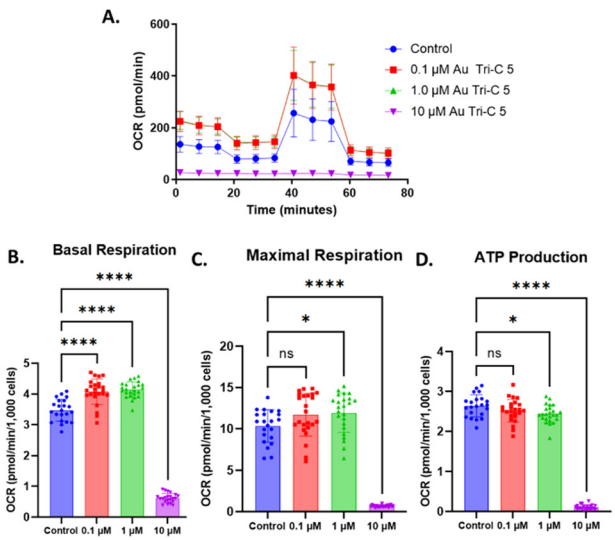

Fig. 6 Mitochondrial bioenergetics assay of BT333 glioblastoma cells after treatment with **AuTri–C 5**. (A) OCR data measured by Seahorse XF96. (B–D) Extrapolated data from Mitostress test on BT333 glioblastoma cells treated with **AuTri–C 5**. Data are plotted as the mean ± SD (n = 22–24 wells). Data were analyzed *via* two-way ANOVA followed by Dunnett's multiple comparison test (*$p < 0.05$, ****$p < 0.0001$, ns = not significant).

the MitoStress assay to measure the oxygen consumption rate (OCR).

This involved the pneumatic injection or pre-treatment of **AuTri–C 5** into wells containing BT333 cells, after which mitochondrial inhibitors of the electron transport chain (ETC) (oligomycin, rotenone, antimycin A) or uncoupler (carbonyl cyanide 4-(trifluoro-methoxy) phenylhydrazone (CCCP)) were injected. We found that pretreatment of **AuTri–C 5** at low concentrations enhances OCR in BT333 cells but at high concentrations of 10 μM induces dysfunction that ablates bioenergetics (Fig. 6). Studying the acute response of BT333 cells to **AuTri–C 5** shows increased OCR. It is possible that initial effects of **AuTri–C 5** on the ETC drives mitochondrial respiration because of fission activity, which becomes a vulnerability for the cells. A deeper biological characterization beyond the scope of this work will help elucidate this possibility. Overall, our data suggest that **Au Tri–C 5** is a potent Au(I) anti-cancer agent in OXPHOS dependent cell lines.

In vivo tumor inhibition

Promising stability and *in vitro* results regarding the anticancer potential of **AuTri–C 5** in patient-derived GBM cells facilitated studies to explore the efficacy of **AuTri–C 5** to inhibit GBM tumor growth *in vivo*. We employed a GFP-expressing patient-derived glioblastoma stem cells (GSCs), G9pCDH for the mouse model, given their dependence on OXPHOS. Briefly, G9pCDH GBM stem cells were injected subcutaneously into the left flank region of BALB/c nude mice. Tumor-bearing mice were randomized based on tumor size as measured by fluorescence and calipers into different groups. The mice were injected with the vehicle or **AuTri–C 5** twice a

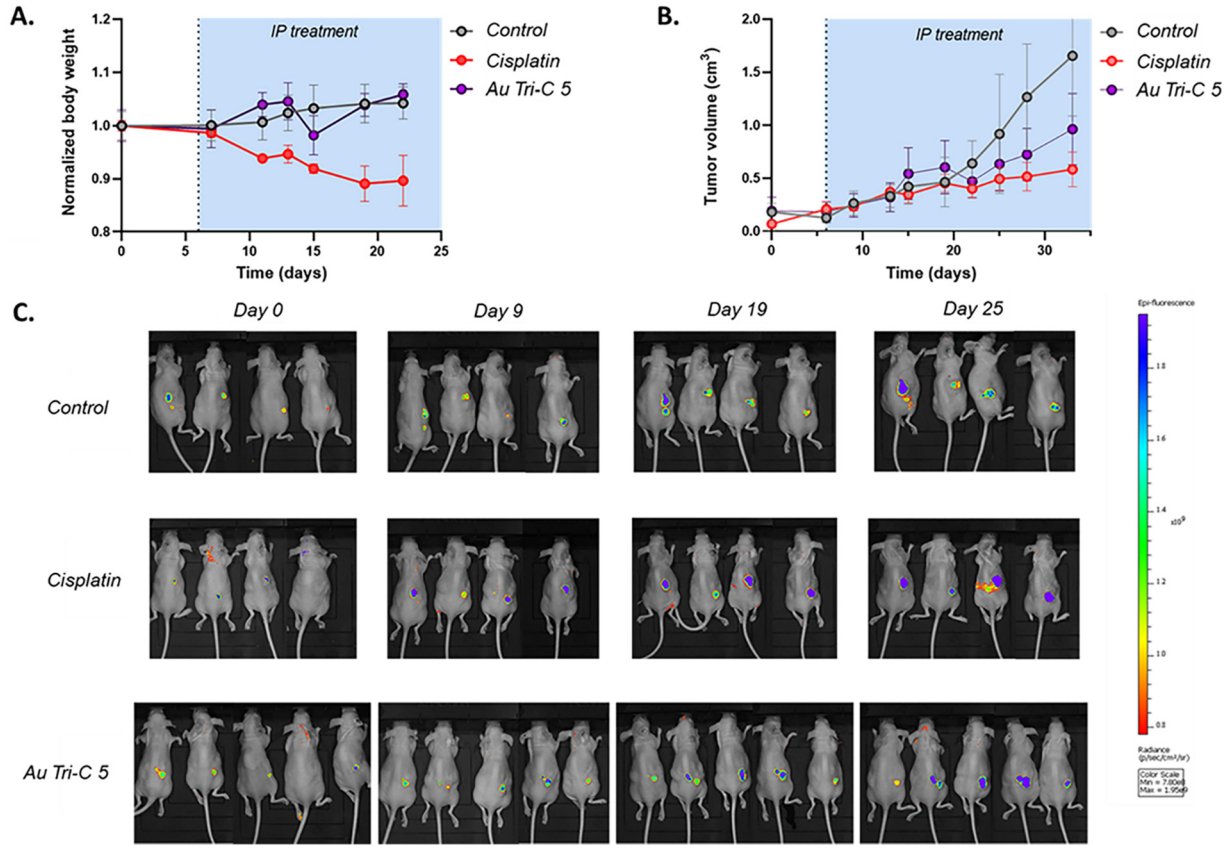

Fig. 7 Therapeutic impact of **AuTri–C 5** in glioblastoma. (A) The change in body weight of **AuTri–C 5** – cisplatin- or vehicle-treated mice over 20 days. (B) The change in tumour volume of G9pCDH stem cell line-bearing mice (300 000 cells inoculated, n = 4 or 5) over 30 days, following intraperitoneal administration of **AuTri–C 5** (16.7 mg kg^{-1}), cisplatin (3 mg kg^{-1}) or the vehicle twice a week. (C) *In vivo* epifluorescence imaging of the control and treated mice at representative time points.

week *via* intraperitoneal injection at a dose equivalent to 16.7 mg kg^{-1} for 28 days. Measurements of the tumor volume showed a significant decrease after treatment when compared to the control (Fig. 7). In addition, mouse body weight was stable over the 28 day treatment time, unlike cisplatin (3 mg kg^{-1}), which induced a 10% decrease in body weight, indicating impressive tolerability of **AuTri–C 5**. Further dose optimization could lead to a larger decrease in tumor volume. Overall, our data suggests that **AuTri–C 5** is a potent Au(I) anti-GBM agent *in vitro* and *in vivo*.

Conclusions

Glioblastoma multiforme (GBM) is extraordinarily deadly and treatment resistant, leading to the necessity of new chemotherapeutic agents. Current treatment plans include resection and radiation therapy, both yielding significant side effects and limited remission. Current research suggests a heavy dependency on oxidative phosphorylation (OXPHOS). The reliance of GBM on mitochondrial respiration provides an opportune therapeutic target.

Herein, we developed and characterized novel cationic Au(I)-based anticancer agents targeting mitochondrial morphology for use in glioblastoma multiforme. To the best of our knowledge, this work is the first report of a Au(I) anti-GBM agent, targeting mitochondrial function. We observed a significant increase in apoptotic cells after treatment with the lead complex **AuTri–C 5**, clear fragmentation of the mitochondria after treatment, significant depolarization of the mitochondrial membrane and alteration of mitochondrial bioenergetics. We also observed a significant decrease in *in vivo* tumor volume in a G9pCDH stem cells tumor mouse model and impressive tolerability by **AuTri–C 5** when compared to the cisplatin positive control.

In summary, we present a novel class of Au(I)-based anti-GBM agents with great promise. A facile synthetic method to prepare these complexes offers a robust platform for optimization and other bioorthogonal-inspired target engagement studies. Additionally, we provide new tools for mitochondrial biology as well as GBM research.

Ethics

All animal experiments were performed in compliance with the relevant laws and institutional guidelines. The procedures described in this study were approved by Brigham and Women's Institutional Animal Care and Use Committee (IACUC).

Author contributions

S. G. A. conceptualized the project. C. E. G. led the project and performed most of the experiments. C. E. G., R. T. M., and S. G. A., worked on the synthetic modification of the parent compound used in this study. G. B. carried out animal studies. C. E. G. and R. T. M. performed flow cytometry and confocal microscopy experiments. C. E. G. wrote the manuscript with guidance from S. G. A. S. G. A. revised the manuscript before submission.

Conflicts of interest

Samuel G. Awuah reports that financial support was provided by University of Kentucky. Samuel G. Awuah reports a relationship with University of Kentucky that includes funding grants. Samuel G. Awuah has patents pending in the University of Kentucky Research Foundation.

Acknowledgements

We thank all the core facilities at the University of Kentucky who provided support in completion of the experiments detailed in this manuscript. Specifically, the UK NMR Center supported by NSF (CHE-997738) and the flow cytometry and immune function core supported by the Office of the Vice President of Research, the Markey Cancer Center, and NCI Center Core Support Grant (P30 CA177558), and the microscopy facilities (UK Light Microscopy Core) for their assistance. We thank Dr. Tomoko Sengoku and Mr. Michael Alstott for their support with our redox metabolism experiments, supported by the shared resource(s) of the University of Kentucky Markey Cancer Center (P30CA177558). This work was funded by National Institutes of Health/NCI grant R01CA258421-01 (S. G. A.).

References

1 M. Lim, Y. Xia, C. Bettegowda and M. Weller, *Nat. Rev. Clin. Oncol.*, 2018, **15**, 422–442.
2 A. Vollmann-Zwerenz, V. Leidgens, G. Feliciello, C. A. Klein and P. Hau, *Int. J. Mol. Sci.*, 2020, **21**, 1932.
3 A. Fukuda, Y. Okuma, T. Hakozaki, K. Mirokuji, M. Yomota, T. Hishima and Y. Hosomi, *Front. Oncol.*, 2022, **11**, 779700.
4 Z. Wu, W. S. Ho and R. Lu, *NeuroMol. Med.*, 2022, **24**, 18–22.
5 D. Sighel, M. Notarangelo, S. Aibara, A. Re, G. Ricci, M. Guida, A. Soldano, V. Adami, C. Ambrosini, F. Broso, E. F. Rosatti, S. Longhi, M. Buccarelli, Q. G. D'Alessandris, S. Giannetti, S. Pacioni, L. Ricci-Vitiani, J. Rorbach, R. Pallini, S. Roulland, A. Amunts, I. Mancini, A. Modelska and A. Quattrone, *Cell Rep.*, 2021, **35**, 109024.
6 A. M. van der Bliek, Q. Shen and S. Kawajiri, *Cold Spring Harbor Perspect. Biol.*, 2013, **5**, a011072.
7 B. Westermann, *Nat. Rev. Mol. Cell Biol.*, 2010, **11**, 872–884.
8 M. Yu, N. D. Nguyen, Y. Huang, D. Lin, T. N. Fujimoto, J. M. Molkentine, A. Deorukhkar, Y. A. Kang, F. A. San Lucas, C. J. Fernandes, E. J. Koay, S. Gupta, H. Ying, A. C. Koong, J. M. Herman, J. B. Fleming, A. Maitra and C. M. Taniguchi, *JCI Insight*, 2019, **4**, e126915.
9 R. T. Mertens, W. C. Jennings, S. Ofori, J. H. Kim, S. Parkin, G. F. Kwakye and S. G. Awuah, *JACS Au*, 2021, **1**, 439–449.
10 R. T. Mertens, S. Parkin and S. G. Awuah, *Chem. Sci.*, 2020, **11**, 10465–10482.
11 M. M. Anastacio, E. M. Kanter, C. Makepeace, A. D. Keith, H. Zhang, R. B. Schuessler, C. G. Nichols and J. S. Lawton, *Circulation*, 2013, **128**, 10.1161.
12 Y. Eura, N. Ishihara, S. Yokota and K. Mihara, *J. Biochem.*, 2003, **134**, 333–344.
13 G. Favaro, V. Romanello, T. Varanita, M. Andrea Desbats, V. Morbidoni, C. Tezze, M. Albiero, M. Canato, G. Gherardi, D. De Stefani, C. Mammucari, B. Blaauw, S. Boncompagni, F. Protasi, C. Reggiani, L. Scorrano, L. Salviati and M. Sandri, *Nat. Commun.*, 2019, **10**, 2576.
14 W. Kühlbrandt, *BMC Biol.*, 2015, **13**, 89.
15 G. J. Hermann, J. W. Thatcher, J. P. Mills, K. G. Hales, M. T. Fuller, J. Nunnari and J. M. Shaw, *J. Cell Biol.*, 1998, **143**, 359–373.
16 C. Olelewe and S. G. Awuah, *Curr. Opin. Chem. Biol.*, 2023, **72**, 102235.
17 C. Olelewe, J. H. Kim, S. Ofori, R. T. Mertens, S. Gukathasan and S. G. Awuah, *iScience*, 2022, **25**, 104340.
18 J. Zhang, Y. Li, R. Fang, W. Wei, Y. Wang, J. Jin, F. Yang and J. Chen, *Front. Pharmacol.*, 2022, **13**, 1–19.
19 K. Sztandera, M. Gorzkiewicz and B. Klajnert-Maculewicz, *Mol. Pharmaceutics*, 2019, **16**, 1–23.
20 C. I. Yeo, K. K. Ooi and E. R. T. Tiekink, *Molecules*, 2018, **23**, 1410.
21 L. Vela, M. Contel, L. Palomera, G. Azaceta and I. Marzo, *J. Inorg. Biochem.*, 2011, **105**, 1306–1313.
22 S. Sen, S. Hufnagel, E. Y. Maier, I. Aguilar, J. Selvakumar, J. E. DeVore, V. M. Lynch, K. Arumugam, Z. Cui, J. L. Sessler and J. F. Arambula, *J. Am. Chem. Soc.*, 2020, **142**, 20536–20541.
23 J. Hyun Kim, S. Ofori, R. T. Mertens, S. Parkin and S. G. Awuah, *ChemMedChem*, 2021, **16**, 3222–3230.
24 K. Minori, L. B. Rosa, R. Bonsignore, A. Casini and D. C. Miguel, *ChemMedChem*, 2020, **15**, 2146–2150.
25 B. Wu, X. Yang and M. Yan, *J. Med. Chem.*, 2019, **62**, 7751–7768.
26 L. Wempe, R. Mohamed, J. Warinner, T. Goretsky, M. Avdiushko, J. Kim, A. Abomhya, G. Lee, S. Awuah, T. Barrett and N. Kapur, *Gastroenterology*, 2022, **162**, S2.
27 R. T. Mertens, S. Gukathasan, A. S. Arojojoye, C. Olelewe and S. G. Awuah, *Chem. Rev.*, 2023, **123**(10), 6612–6667.
28 G. Moreno-Alcántar, P. Picchetti and A. Casini, *Angew. Chem., Int. Ed.*, 2023, **135**, e202218000.
29 T. Zou, J.-J. Zhang, B. Cao, K.-C. Tong, C.-N. Lok and C.-M. Che, *Isr. J. Chem.*, 2016, **56**, 825–833.
30 T. Zou, C. T. Lum, C.-N. Lok, J.-J. Zhang and C.-M. Che, *Chem. Soc. Rev.*, 2015, **44**, 8786–8801.
31 J. H. Kim, S. Ofori, S. Parkin, H. Vekaria, P. G. Sullivan and S. G. Awuah, *Chem. Sci.*, 2021, **12**, 7467–7479.
32 C. K. Mirabelli, D. T. Hill, R. K. Johnson, L. F. Faucette, C. M. Sung, S. T. Crooke, G. R. Girard and G. Y. Kuo, *J. Med. Chem.*, 1986, **29**, 218–223.

33 O. Rackham, S. J. Nichols, P. J. Leedman, S. J. Berners-Price and A. Filipovska, *Biochem. Pharmacol.*, 2007, **74**, 992–1002.
34 P. de Frémont, N. Marion and S. P. Nolan, *J. Organomet. Chem.*, 2009, **694**, 551–560.
35 A. M. Al-Majid, M. I. Choudhary, S. Yousuf, A. Jabeen, R. Imad, K. Javeed, N. N. Shaikh, A. Collado, E. Sioriki, F. Nahra and S. P. Nolan, *ChemistrySelect*, 2017, **2**, 5316–5320.
36 S. Gaillard, C. S. J. Cazin and S. P. Nolan, *Acc. Chem. Res.*, 2012, **45**, 778–787.
37 A. Collado, A. Gómez-Suárez, A. R. Martin, A. M. Z. Slawin and S. P. Nolan, *Chem. Commun.*, 2013, **49**, 5541–5543.
38 Y. Iranmanesh, B. Jiang, O. C. Favour, Z. Dou, J. Wu, J. Li and C. Sun, *Front. Oncol.*, 2021, **11**, 1–11.
39 M. Magalhães, E. M. Domínguez-Martín, J. Jorge, A. C. Gonçalves, A. M. Díaz-Lanza, B. Manadas, T. Efferth, P. Rijo and C. Cabral, *Front. Pharmacol.*, 2022, **13**, 1–12.
40 A. Nagy, K. Eder, M. A. Selak and B. Kalman, *Brain Res.*, 2015, **1595**, 127–142.
41 H. Chen and D. C. Chan, *Ann. N. Y. Acad. Sci.*, 2010, **1201**, 21–25.
42 E. E. Griffin, S. A. Detmer and D. C. Chan, *Biochim. Biophys. Acta, Mol. Cell Res.*, 2006, **1763**, 482–489.
43 J. N. Meyer, T. C. Leuthner and A. L. Luz, *Toxicology*, 2017, **391**, 42–53.
44 B. Perillo, M. Di Donato, A. Pezone, E. Di Zazzo, P. Giovannelli, G. Galasso, G. Castoria and A. Migliaccio, *Exp. Mol. Med.*, 2020, **52**, 192–203.
45 S. P. Totten, Y. K. Im, E. Cepeda Cañedo, O. Najyb, A. Nguyen, S. Hébert, R. Ahn, K. Lewis, B. Lebeau, R. La Selva, V. Sabourin, C. Martínez, P. Savage, H. Kuasne, D. Avizonis, N. Santos Martínez, C. Chabot, A. Aguilar-Mahecha, M.-L. Goulet, M. Dankner, M. Witcher, K. Petrecca, M. Basik, M. Pollak, I. Topisirovic, R. Lin, P. M. Siegel, C. L. Kleinman, M. Park, J. St-Pierre and J. Ursini-Siegel, *Nat. Commun.*, 2021, **12**, 3299.
46 M. Sundqvist, K. Christenson, H. Björnsdottir, V. Osla, A. Karlsson, C. Dahlgren, D. P. Speert, A. Fasth, K. L. Brown and J. Bylund, *Front. Immunol.*, 2017, **8**, 1–11.
47 M. Y. Vyssokikh, S. Holtze, O. A. Averina, K. G. Lyamzaev, A. A. Panteleeva, M. V. Marey, R. A. Zinovkin, F. F. Severin, M. V. Skulachev, N. Fasel, T. B. Hildebrandt and V. P. Skulachev, *Proc. Natl. Acad. Sci. U. S. A.*, 2020, **117**, 6491–6501.
48 D. B. Zorov, M. Juhaszova and S. J. Sollott, *Physiol. Rev.*, 2014, **94**, 909–950.
49 P. Mukhopadhyay, M. Rajesh, K. Yoshihiro, G. Hasko and P. Pacher, *Biochem. Biophys. Res. Commun.*, 2007, **358**, 203–208.